Calibrating Time-variant, Device-specific Phase Noise for COTS WiFi Devices

Jincao Zhu
University of Colorado Boulder
Boulder, Colorado
jincao.zhu@colorado.edu

Youngbin Im
University of Colorado Boulder
Boulder, Colorado
youngbin.im@colorado.edu

Shivakant Mishra
University of Colorado Boulder
Boulder, Colorado
shivakant.mishra@colorado.edu

Sangtae Ha
University of Colorado Boulder
Boulder, Colorado
sangtae.ha@colorado.edu

ABSTRACT

Current COTS WiFi based work on wireless motion sensing extracts human movements such as keystroking and hand motion mainly from amplitude training to classify different types of motions, as obtaining meaningful phase values is very challenging due to time-varying phase noises occurred with the movement. However, the methods based only on amplitude training are not very practical since their accuracy is not environment and location independent. This paper proposes an effective phase noise calibration technique which can be broadly applicable to COTS WiFi based motion sensing. We leverage the fact that multi-path for indoor environment contains certain static paths, such as reflections from wall or static furniture, as well as dynamic paths due to human hand and arm movements. When a hand moves, the phase value of the signal from the hand rotates as the path length changes and causes the superposition of signals over static and dynamic paths in antenna and frequency domain. To evaluate the effectiveness of the proposed technique, we experiment with a prototype system that can track hand gestures in a non-intrusive manner, i.e. users are not equipped with any device, using COTS WiFi devices. Our evaluation shows that calibrated phase values provide much rich, yet robust information on motion tracking – 80th percentile angle estimation error up to 14 degrees, 80th percentile tracking error up to 15 cm, and its robustness to the environment and the speed of movement.

CCS CONCEPTS

• **Hardware → Digital signal processing**; **Wireless devices**; *Sensor devices and platforms*;

KEYWORDS

Phase calibration; Wireless sensing; Central frequency offset; CFO; COTS WiFi

SenSys'17, November 6–8, 2017, Delft, The Netherlands

ACM ISBN 978-1-4503-5459-2/17/11.
https://doi.org/10.1145/3131672.3131695

ACM Reference Format:
Jincao Zhu, Youngbin Im, Shivakant Mishra, and Sangtae Ha. 2017. Calibrating Time-variant, Device-specific Phase Noise for COTS WiFi Devices. In *Proceedings of 15th ACM Conference on Embedded Networked Sensor Systems (SenSys'17).* ACM, New York, NY, USA, 12 pages. https://doi.org/10.1145/3131672.3131695

1 INTRODUCTION

Human motion and position tracking are the core technologies enabling a wide range of useful applications, including health care, smart home, security, gaming, and so on. As a result, there is a large body of research addressing this problem. This includes training-based, sensor-based which uses built-in sensors such as accelerometer and gyroscope [18], and signal-variation based technologies [10] that rely on variations in different characteristics of a signal, e.g. amplitude to detect motion. A key limitation of sensor-based technologies is that they require the users to be equipped with sensor devices, e.g. smartphones or wearables, and hence are intrusive in nature. Prior work in signal-variation based technologies has investigated the possibility of leveraging several different types of signals, such as acoustic signal [13, 24], visual light signal [4], Kinect [1], and Leapmotion [12] for human motion sensing and tracking. In particular, radio frequency (RF) based sensing technologies have gained significant attention recently due to the advantage of RF being able to penetrate objects over other types of signals, and thus work in non-line-of-sight (NLOS) situations.

RF-based sensing technologies can be divided into two categories, RF-based active sensing, and RF-based passive sensing. The RF-based active sensing [21] is intrusive in nature since users must carry one or more RF devices. The RF-based passive sensing, on the other hand, does not require users to be equipped with any device and hence is non-intrusive in nature, and thus is more attractive. However, building an RF-based passive sensing technology is very challenging. One category of RF-based passive sensing technologies is to make use of dedicated devices such as software-defined radios (SDRs). For example, [3] allows a user to track moving humans through walls and behind closed doors using WiFi signals, [2] uses SDR to generate the wide band frequency-modulated continous wave (FMCW) signal to detect a human, and WiDeo [7] shows the possibility of fine-grained motion tracking with WiFi technology. Another category is to use commercial-off-the-shelf (COTS) WiFi devices for RF-based passive sensing. Because of the high

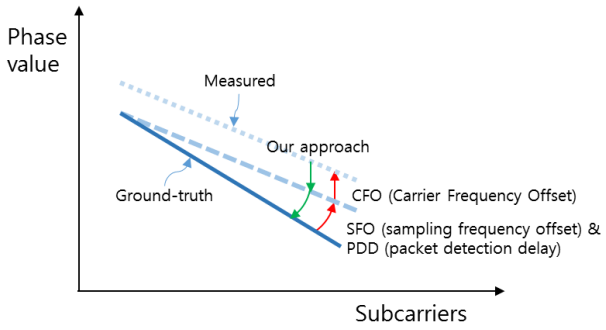

Figure 1: Phase noise consisting of SFO, PDD, and CFO is added to the ground-truth signal.

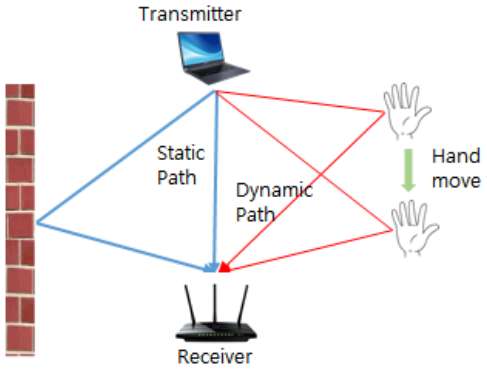

Figure 2: Dynamic path is created when a hand moves while static path does not change.

cost of dedicated SDR devices, leveraging the COTS WiFi device is much more attractive since WiFi NIC cards are much cheaper, more pervasive and easily available. Indeed, researchers have begun to investigate WiFi NIC cards for passive sensing.

With Channel State Information (CSI) [5] obtained from COTS WiFi devices, several interesting applications ranging from localization [8] to sensing [9] and activity tracking [10] have been developed. A key limitation of these applications is that they rely mostly on training with amplitude values, since it is very difficult to extract clean phase values in the presence of extreme phase noise from cheap WiFi NIC cards with poor oscillators. For example, [9, 19] and [10] recognize human heartbeats and keystrokes, respectively, through training the amplitude values of the CSI. As a result, these methods are not time and environment consistent [10]. Even a slight change in the direction or location of the user may require an additional cycle of training, which is time consuming and impractical.

Although some of the recent works [16, 19] are not training based, they have their own limitations. For example, WiDraw [16] harnesses the Angle-of-Arrival (AoA) values of incoming wireless signals at the mobile device to track the user's hand trajectory with a large number of APs (30 Tx/Rx in their experiment) surrounding the mobile device. The method proposed in [19] to measure the human respiration using the COTS WiFi device is only applicable to small, regular movement like respiration (i.e, one directional movement), and cannot be used to track more complex motions such as hand movement. CARM [23] uses the CSI change speed to detect simple push and pull-type motions, not complex ones.

Because of the phase noise occurring during the movement, none of the existing work using COTS WiFi devices leverage the phase values except SpotFi [8]. However, the method used by SpotFi [8] for device localization cannot be used for passive sensing. SpotFi deals only with static paths and finds the best linear fit of the unwrapped CSI phase to eliminate the phase noise due to Sampling Frequency Offset (SFO). Thus there is no need to calibrate the Central Frequency Offset (CFO). Chronos [17], on the other hand, requires to measure the CSI on the both side of the link to eliminate the CFO, which needs modification of the driver of WiFi NIC to piggy back the CSI on each side.

Challenges. We briefly describe the challenges of using the COTS WiFi devices for RF-based passive sensing:

- The first challenge of COTS WiFi is the presence of phase noise. As shown in Figure 1, the phase noise includes the SFO, Packet Detection Delay (PDD) and CFO, which are time variant across different devices. SFO and PDD have the same effect and we use SFO to present SFO and PDD. Unlike the SFO and PDD which vary over two CSI matrices (i.e., vary over time), the CFO has the *same random phase shift across subcarriers and antennas*. As a result, we are not able to extract the CSI change by subtracting two CSI matrices. Our question is then how can we calibrate the CFO to extract the ground-truth.
- The second challenge is related to the strong power of a static path, which makes it hard to extract the weak path signal created with movement. Figure 2 shows the dynamic path created during hand movement. In this case, we do not have the resolution of every path of the channel, and as a result, the final path resolution may mix the dynamic path with static paths.
- The third challenge is with the limited number of antennas. In order to achieve good resolution, Wideo [7] uses a large number of antenna arrays using SDR. This would result in a bulky and expensive device. Furthermore, common COTS WiFi NIC cards only have three antennas at the most.

Our approach. To effectively deal with the phase noise over dynamic path (mentioned in the first challenge), we leverage the phenomenon of sinusoid wave on amplitude and phase values upon the dynamic path length change. To remove phase noise and calibrate the CFO of the CSI for dynamic path when a motion occurs, we first extract the amplitude of dynamic path. Then we get the dynamic path CSI phase difference according to the triangle relationship of measured CSI, static path CSI vector and dynamic path CSI vector. The method extracting the dynamic path from the static path also solves the second challenge. Note that although [24] also extracts dynamic path with acoustic signals, it does not need to deal with the phase noise due to CFO, resulting in its limited applicability to COTS WiFi devices. To deal with the third challenge, we combine both frequency and antenna domains to increase the accuracy, which is inspired from SpotFi [8].

Contributions. To the best of our knowledge, this is the first work that calibrates the CFO to remove the phase noise occurred with movement on COTS WiFi devices. By removing the phase noise, we are able to use both amplitude and phase values that occur with human movement, and therefore no training is needed to classify different movements. Moreover, the proposed method can obtain the information of dynamic path by removing the information of static path, enabling more environment independent applications. This method is general enough that it can be used for several existing COTS WiFi-based sensing and tracking applications. As a proof-of-concept of exploiting this CFO calibration, we prototype a system that tracks human hands gestures, which are 2D motions.

In summary, our contributions are as follows:

(1) We propose a method to effectively calibrate the COTS WiFi phase noise when there is a dynamic path with movement.
(2) To demonstrate the effectiveness of the proposed phase noise cancellation, we design and implement the prototype of a 2D hand tracking system with COTS WiFi devices, and show that the system can effectively isolate the CSI of dynamic path from the noisy CSI measured.

Our evaluation with the prototype shows that calibrated phase values provide much rich, yet robust information on motion tracking; the tracking accuracy is robust to the environment and the speed of movement while providing fine-grained tracking accuracy.

The rest of the paper is organized as follows. In Section 2, we provide a summary of the related work. Then we briefly describe the background of some of the key wireless technologies that we have used in this paper in Section 3. Section 4 explains how we calibrate CSI phase noise, while Section 5 describes the design of our prototype system. We present the implementation and evaluation of our prototype in Section 6. We discuss the limitations of the proposed approach in Section 7, before concluding the paper in Section 8.

2 RELATED WORK

Non-RF based motion tracking. Motion tracking has drawn a lot of attention from research communities. Sensor-based motion detection [1, 12] has been widely used in games, but it requires use of dedicated devices. Vision or light based motion tracking uses light sensors or cameras to track human gesture or movement [4]. Such systems require line-of-sight setup from the device to the subject. Acoustic signal based sensing is attractive because of its short wavelength providing higher accuracy on measurements. [13, 24] use acoustic signals generated by cell phone to track hand movement with an accuracy of 3.5 mm. [11] uses a cellphone as the mouse over the air by letting it measure the sound generated by the speakers deployed nearby. However, acoustic signals do not work in non-line-of-sight scenarios.

RF-based Active sensing. Both RF-IDraw [21] and Tagoram [27] use RFID for tracking purpose. The advantage is that the tag is low cost and battery free. However, these systems require a dedicated RFID reader, which is expensive. RF-IDraw can achieve centimeter-level accuracy while Tagoram achieves an accuracy of less then 1cm. The COTS WiFi based system is cheaper and more pervasive than RFID-based systems. SpotFi [8] and Chronos [17] calibrate the phase of static CSI in order to track a wireless node. However, such methods can not be used when there are moving objects around the subject, since the dynamic path CSI is not extracted from the measured CSI.

Table 1: RF-based sensing technologies

Work	Training?	SDR/COTS	Active?
RF-IDraw [21]	No	RFID	Active
Matrack [25]	No	SDR(60GHz)	Passive
WiDeo [7]	No	SDR	Passive
SpotFi [8]	No	COTS	Active
Respiration [19]	Yes	COTS	Passive
CARM/Wikey [10, 23]	Yes	COTS	Passive
WiDraw [16]	No	30 COTS	Passive
Widir [26]	No	COTS	Passive
LiFS [20]	No	COTS	Passive
Gait [22]	No	COTS	Passive

RF-based Passive sensing. Device-free sensing provides more flexibility, so is more attractive. Tadar [28] uses RFID tags as an antenna array and tracks indoor activity from a location separated by a wall in between. mTrack [25] can track small movements like a pen movement by using millimeter wave of 60 Ghz. Wideo [7] provides a highly precise tracking capability with WiFi technology, but uses SDR, which makes it more difficult to deploy compared to the COTS WiFi devices.

The COTS WiFi platform is more attractive due to its low price and high availability of components compared to non-COTS based solutions. We can divide COTS WiFi based passive tracking solutions into two categories, training-based and non-training-based. Training based solutions leverage machine learning to identify different motions or activities by measuring the pattern of CSI change. Wikey [10] is able to identify key stroking with high accuracy. Gait [22] can extract human walking patterns to identify different persons. However, training-based solutions have one key drawback. They are highly dependent on training and are highly environment dependent. Thus, these solutions require completely new training whenever there is an even slight change in the environment.

Non-training based solutions, on the other hand, do not require training. For example, [19] can detect respiration movement with some constraints on human body orientation and relative position to the WiFi nodes. Widir [26] can track human walking direction by analyzing phase change dynamics from multiple WiFi subcarriers. LiFS [20] uses power fading model to passively localize human using the fact that human body blocks WiFi signal in different ways at different locations. CARM [23] models the path length change using signal amplitude fluctuations and uses the CSI-speed model to map the path length changes to different activities. However, none of these approaches can extract dynamic path CSI from the measured CSI for a finer grained sensing, such as human hand movement tracking. Although Widraw [16] is able to track a human hand for an application like drawing, its precision is restrictively dependent on the high density deployment of wireless access points. We summarize the related work using RF-based sensing in Table 1.

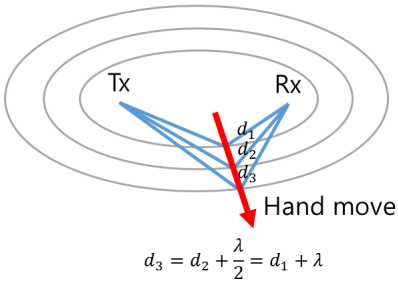

Figure 3: A reflector crossing Fresnel zones in one direction is illustrated. When a hand moves, the distance from TX/RX to the hand increases by half λ (2.6cm for 5GHz, and 5cm for 2.4GHz).

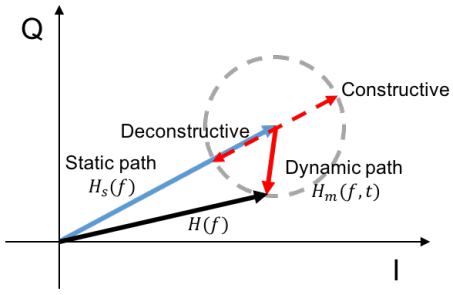

Figure 4: Superposition of signals over static paths and dynamic paths is illustrated. Whether the signals are added constructively or destructively is decided by the relative phase differences between these signals.

3 BACKGROUND AND OBSERVATION

In this section, we describe the background of the wireless technologies we have used. In particular we present key observations and describe how the amplitude and phase values of CSIs measured in consecutive period of time can be used in calibrating phase noise.

3.1 CSI measurements

Today's WiFi radios use Orthogonal Frequency-Division Multiplexing (OFDM) modulation and transmit signals across orthogonal subcarriers at different frequencies. Each transmitted symbol $X(f,t)$ is modulated on a subcarrier index f at time t, and the received symbols vector for a receiving antenna array is $Y(f,t) = [Y_1(f,t), Y_2(f,t), ..., Y_M(f,t)]^\top$, where $Y_i(f,t)$ is the received symbol on i^{th} antenna, and M is number of antennas. $Y(f,t)$ depends on the wireless spatial channel $H(f,t)$:

$$\begin{aligned} Y(f,t) &= H(f,t)X(f,t) \\ H(f,t) &= [H_1(f,t), H_2(f,t), ..., H_M(f,t)]^\top \end{aligned} \tag{1}$$

The CSI matrix reported by a WiFi NIC at time t is the estimation of $H(f,t)$ over different frequencies f (i.e., subcarriers) for an antenna array, meaning the columns correspond to the estimated spatial channel vector $H(f,t)$ for different subcarriers:

$$\begin{aligned} CSI^{MN} &= [H(1,t), H(2,t), ..., H(N,t)] \\ &= \begin{bmatrix} H_1(1,t) & H_1(2,t) & \dots & H_1(N,t) \\ H_2(1,t) & H_2(2,t) & \dots & H_2(N,t) \\ \vdots & \vdots & \ddots & \vdots \\ H_M(1,t) & H_M(2,t) & \dots & H_M(N,t) \end{bmatrix} \end{aligned} \tag{2}$$

When multiple paths co-exist, H can be expressed as a summation of all the paths, which is called wave superposition:

$$\begin{aligned} H(f,t) &= \sum_{l=1}^{L} [a_l(t)\, e^{-j2\pi f \tau_l(t)} \times \Phi_l] \\ \Phi_l &= \begin{bmatrix} 1 \\ e^{-j2\pi d cos(\alpha_l)} \\ e^{-j2\pi 2 d cos(\alpha_l)} \\ \vdots \\ e^{-j2\pi(M-1) d cos(\alpha_l)} \end{bmatrix} \end{aligned} \tag{3}$$

In other words, there will be a $e^{-j2\pi(m-1)dcos(\alpha_l)}$ phase shift for the m^{th} antenna on path l which has AoA of α_l, where a_l, τ_l represent the attenuation and time of flight of path l, respectively. A receiver receives the combination of reflections from multiple regions in space at each of its antennas, and signals with different wavelengths over different paths cancel/strengthen each other.

However, the measured CSI contains the SFO and CFO, which make the CSI values look random. The offset is expressed as: $-2\pi f_\delta (n-1)\tau_s - 2\pi f_{\Delta_c}$ on the n^{th} subcarrier, where f_δ is the bandwidth between two adjacent subcarriers in the reported CSI for the NIC, τ_s and f_Δ are the PDD+1/SFO and CFO, respectively. Therefore, the measured CSI at the subcarrier f is:

$$\tilde{H}(f) = H(f) e^{-2\pi f_\delta (n-1)\tau_s - 2\pi f_{\Delta_c}} \tag{4}$$

As shown in Eq. 4, the measured CSI does not provide the correct phase value of the channel, but the amplitude and phase difference across antennas is still reliable.

3.2 CSI amplitude changes

On the commodity WiFi devices, the CSI can be exported by leveraging the open source CSI tool[5]. For example, on each transmission, a matrix of CSI measurements over 30 subcarriers and 3 antennas is exported by the CSI tool for the Intel 5300 NIC with three receiving antennas.

Governed by the principle of superposition of waves, signals reflected by human motion may add constructively or destructively with WiFi signals traveled through other paths, e.g., the Line-Of-Sight (LOS) path. Identiying whether these WiFi signals are added constructively or deconstructively could be determined by the relative phase difference between these signals.

Such phenomena are a characteristic of Fresnel zone [6]. Fresnel zone (illustrated in Figure 3) is a series of ellipsoidal along which the propagation path length from the transmitter to the reflector then to the receiver is constant. So when the reflector crosses different zones in one direction, the phase value rotates and ends up arriving out of phase or in phase with the static path signal periodically. As

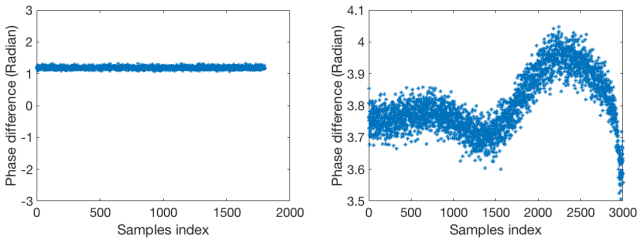

(a) No movement (b) Hand movement

Figure 5: The phase difference between antennas for different scenarios are shown. We observe the significant changes in phase differences when a hand moves.

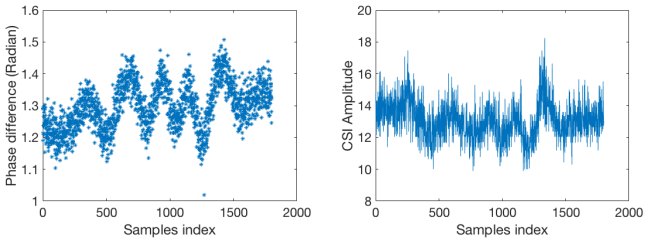

(a) Phase differences (b) Amplitude changes

Figure 6: Phase differences and amplitude changes with push motion.

illustrated in Figure 4, when dynamic path and static path vectors on IQ plane are in the same direction, the amplitude is maximum, while the amplitude is minimum in reverse direction. Such phenomenon is due to the fact that a static path is stable with larger power, and a dynamic path is more dynamic with much weaker power. The static path decides the long term base wave shape, while the dynamic path decides the short time wave shape.

Among previous passive WiFi sensing works, [19] identified each CSI amplitude change cycle in order to obtain a breathing cycle, [26] leverages the frequency diversity of Fresnel zone to identify walking direction, CARM[23] uses a machine learning methodology to classify different human activities, and [22] showed that it can distinguish human gaits. While these works exploit the amplitude change for different sensing applications, we instead compute the relative phase value of dynamic path over static path.

3.3 CSI phase difference

Although the measured CSI phase for individual subcarrier looks totally random due to the phase offset, the phase difference is stable. Through measurement experiments, we observe that the phase difference of a particular subcarrier across different antennas shows distinctive patterns for different movements as shown in Figure 5. We can clearly see how the phase value difference changes according to human breathing and hand movement. PinLoc [15] also leveraged phase difference across multiple subcarriers to obtain location signatures. But their location signatures require mapping and training, while our work is to eliminate the use of training. One important observation is that the phase difference is stable over time with no movement, which means when the phase difference changes significantly, it is mainly due to a movement.

As a result, if we assume that the static path does not change over time (Figure 2), the peak and valley points of CSI amplitude will always have the same phase values with the phase values of the static path. We can use this observation to calibrate the CFO, which is explained in Section 4. Even though there will be a drift over time, as static path will slowly change, such drift is acceptable as long as the dominant path does not change.

4 CSI CALIBRATION

As shown in Figure 2, to track a motion (e.g., hand movement), we first need to extract the dynamic path CSI corresponding to

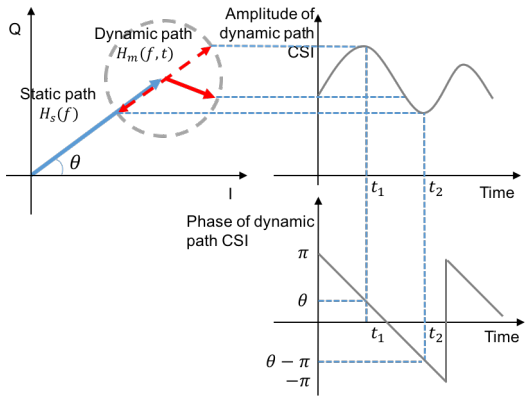

Figure 7: CSI calibration

the motion. Previous work using acoustic signals [24] can not be applied to COTS WiFi signals, as there is no CFO when an acoustic signal is transmitted and received by the speaker and microphone on the same device which share the same oscillator. In our case, while COTS WiFi signals have too much phase noise, we are able to calibrate the phase values of the CSI with dynamic path by leveraging the phase differences and amplitude changes upon a hand move. Then we extract the dynamic path CSI for hand tracking. The steps are illustrated in the following subsections.

4.1 SFO calibration

The SFO is introduced as a linear phase shift across the subcarriers. More specifically, there is a phase shift of $-2\pi f_\delta(k-1)\tau_s$ on subcarrier k, while τ_s is the delay caused by SFO, which varies across packets. We use a linear fit as is done in SpotFi [8]. After this calibration, the linear shift between different subcarriers will be gone and thus free from SFO variations. Note that the phase difference between antennas is not affected by SFO, but the subcarriers are.

4.2 CFO calibration

After SFO calibration, we have to adjust the CFO, which is particularly challenging for dynamic path since the CFO is different for different measurements. The CFO, however, is consistent in one measurement across all subcarriers and across different antennas.

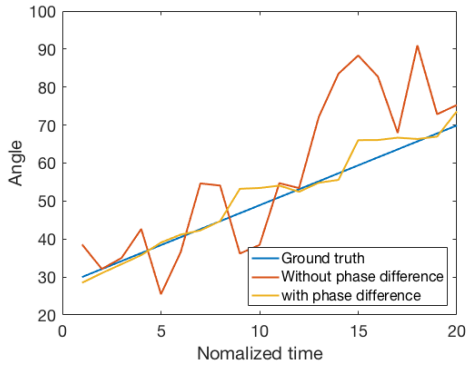

Figure 8: Measurement of dynamic path AoA

Our calibration mechanism is based on two observations. First, when the hand moves in one direction, the path length of dynamic path reflected by the hand will change accordingly. As a result we can observe a sinusoid waved CSI amplitude (Figure 6b) with the unique pattern of phase differences (Figure 6a) between subcarriers. With the assumption that the peak and valley amplitude values are due to the in-phase and out-phase between the static path and the dynamic path, we can say that the phase values of the dynamic path at these two critical points are the same as the ones in the static path. In other words, the phase value where the amplitude is maximum has the same value with the static path, while the phase value where the amplitude is minimum has the phase value of static path minus π (Figure 7). And we could infer the amplitude of the static path and the dynamic path according to this observation and identify the angle between static path vector and dynamic path vector.

Second, in addition to the amplitude fluctuation, we also have the phase difference of measured CSI across antennas and subcarriers. We have the observation that the phase difference across subcarriers and antennas are more reliable than directly calculating phase values of all the subcarriers. Figure 8 shows a comparison of results for the dynamic path AoA estimation algorithm with and without taking phase difference into account. The measured phase difference will significantly improve the accuracy.

In summary, to calibrate the CFO, we first assume that the phase of the static path is constant. We then leverage the amplitude fluctuation to infer the dynamic path amplitude and the triangle relationship between raw CSI vector, static path vector and dynamic path vector. Finally, we get the dynamic path CSI phase difference relative to the reference phase difference of the measured raw CSI.

Algorithm 1 shows the pseudo code of our algorithm which extracts the dynamic path CSI. The algorithm is also illustrated in Figure 9. We first calculate the amplitude of static path and dynamic path according to the fluctuation of measured CSI amplitude, then by comparing phase difference between subcarriers of measured CSI, we get the calibrated phase values for both the static and dynamic paths.

Extracting the amplitude of the dynamic path and static path, respectively. From Figure 4, we can see that the amplitude of the CSI at the maximum point is the summation of the static path amplitude A_s and the dynamic path amplitude A_d, that is, $A^{max} = A_s + A_d$. On the other hand, the minimum CSI amplitude is the difference between A_d and A_s, that is, $A^{min} = A_s - A_d$. If we assume the static path is constant, then by calculating half of the difference between A_{max} and A_{min}, we can get the amplitude of dynamic path, that is $A_d = (A^{max} - A^{min})/2$. In reality, however, the CSI amplitude changes over time and the signals from the static paths are not constant. Therefore, we calculate the amplitude of the static paths by averaging the nearby maximum and minimum points as in Figure 9a. After getting the amplitude of the static paths, we can get the dynamic path amplitude at the peak points (t_1, t_3, t_5, t_7 in Figure 9a) of the CSI wave by: $A_d(t) = A^d(t) - A_s(t)$, and the dynamic path amplitude at the valley points (t_2, t_4, t_6 in Figure 9a) of the CSI wave by: $A_d(t) = A_s(t) - A^{min}(t)$. The dynamic path amplitude of the rest of the samples is calculated by averaging as shown in Figure 9b.

Algorithm 1: Algorithm for extracting the CSI on dynamic path by calibrating the CFO.

Input: SFO calibrated static CSI measured during static time H_s, SFO calibrated CSI: $H(k, f, t)$, k: antenna index $1:K$, f: subcarrier index $1:F$, $t = 1:T$ is sample index
Output: H_d, $C\hat{F}O$
Initialize: α: the smooth average parameter, $[X(k, f, n)\ l(k, f, n)]$ list of amplitude extreme point and sample index, n=0;
/* get amplitude of dynamic path and static component*/
for *each subcarrier stream (k,f)* **do**
  $A(t) = |H(k, f, t)|$;
  for *t = 1 to T* **do**
    if $A(t)$*is a local maxima or minima* **then**
      n=n+1;
      E(n)=A(t);
      $A_{st}(n) = (E(n-1) + E(n))/2$;
      $A_{dt}(n) = |E(n-1) - E(n)|/2$;
    /*smooth averaging */
    $A_s(t) = (1-\alpha)A_s(t-1) + \alpha A_{st}(n)$;
    $A_d(t) = (1-\alpha)A_d(t-1) + \alpha A_{dt}(n)$;
    /*angle between static path vector and measured channel vector */
    $\theta_s = arg(cos((A^2 + A_s^2 - A_d^2)/(2A * A_s))$;
    /*angle between dynamic path vector and measured channel vector */
    $\theta_d = arg(cos((A^2 + A_d^2 - A_s^2)/(2A * A_d))$;
    /*first subcarrier stream*/
    if *((k,f)==(1,1))* **then**
      $p_{base}(t) = \theta_s$;
    $p_d(t) = \angle(H(k, f, t), H(1, 1, t)) + p_{base}(t) - \theta_d$;
    /*Get the intermediate estimated dynamic dynamic path CSI $H_d^{'}$ */
    $H_d^{'}(k, f, t) = A_d(t) * exp(-jp_d(t))$;
for *t = 1 to T* **do**
  $C\hat{F}O(t) = \arg\min_{CFO} \left\| H(t) - H_s \times CFO - H_d^{'}(t) \right\|$;
  $H_d(t) = H(t) - H_s \times C\hat{F}O(t)$;
return H_d, $C\hat{F}O$;

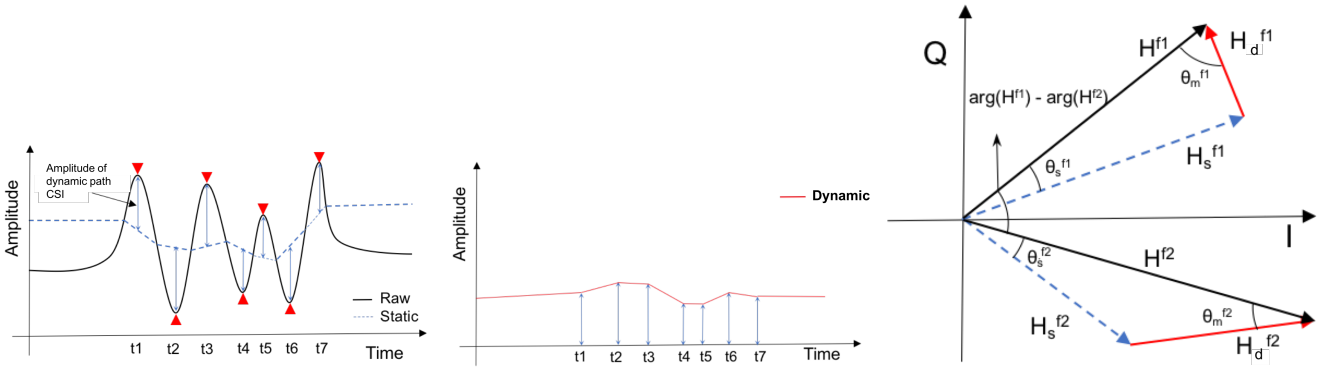

(a) Calculation of the amplitude of static paths (b) Calculation of the amplitude of dynamic path (c) Phase difference between the two subcarriers of dynamic path

Figure 9: Dynamic path CSI calculation

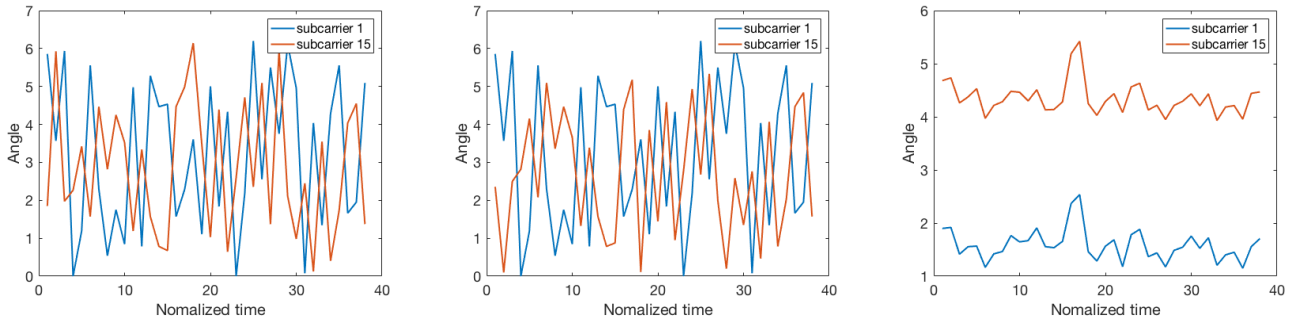

(a) Original phase (b) Phase values after SFO calibration (c) Phase values after CFO calibration

Figure 10: Phase calibration

Calculating the angle of measured raw CSI vector and the dynamic path vector, respectively. At IQ plot of an individual subcarrier, the raw CSI vector is the addition of the static component vector and the dynamic path vector as in Figure 9c: $H = H_s + H_d$. At this point, we already have the amplitude of the raw CSI vector $A = |H|$, static component vector $A_s = |H_s|$, and dynamic path vector $A_d = |H_d|$. So we can get the relative angle of raw CSI vector and the dynamic path vector, respectively, as: $\theta_s = arg(cos((A^2 + A_s^2 - A_d^2)/(2A * A_d))$ and $\theta_d = arg(cos((A^2 + A_d^2 - A_s^2)/(2A * A_d))$ in Figure 9c.

Calibration phase. To calculate the Angle of Arrival (AoA) of the dynamic path, we need the phase difference of dynamic path across antennas and subcarriers. For each pair of subcarriers, we calculate the phase difference of the dynamic path. In Figure 9c, we have two subcarriers $f1$ and $f2$. We have the raw CSI measurements H^{f1} for $f1$ and H^{f2} for $f2$. Although the CSI measurements do not provide the absolute phase value for $f1$ and $f2$, respectively, due to the CFO, the phase difference $arg(H^{f1}) - arg(H^{f2})$ is still preserved in our extensive measurements. By observing the raw CSI amplitude fluctuation we get the amplitude of static paths and dynamic path as in Figures 9a and 9b. And further, we can have the angle of raw CSI vector and dynamic path vector in Figure 9c, θ_d^{f1} for subcarrier $f1$ and θ_d^{f2} for subcarrier $f2$. So we can calculate the phase difference of the dynamic path:

$$p_d^{(f1,f2)} = \angle(H^{f1}, H^{f2}) + \theta_d^{f1} - \theta_d^{f2} \tag{5}$$

And we already have the CSI of statistic paths with SFO removed, can be represented as H_s. $H_d^{'}$ is the CSI of dynamic path which can be calculated with amplitude and phase difference obtained. So the CFO can be calculated as:

$$\hat{CFO}(t) = \arg\min_{CFO} \left\| H(t) - H_s \times CFO - H_d^{'}(t) \right\| \tag{6}$$

Then our final estimation of dynamic path H_d is:

$$H_d(t) = H(t) - H_s \times \hat{CFO}(t) \tag{7}$$

To validate our idea, we experiment our algorithm with WiFi signals. Figure 10 shows how phase values change with our calibration techniques when we push and pull the hand. We can see that the phase values of subcarriers 1 and 2 are quite noisy even after the SFO calibration. With the CFO calibration, however, the phase values of subcarriers 1 and 2 become quite similar. This makes sense

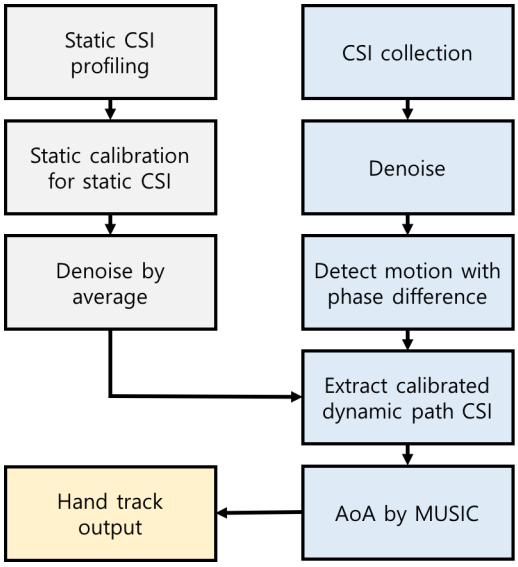

Figure 11: System Architecture

given that subcarriers in the channel will be affected very similarly upon a particular hand movement.

Note that our phase calibration is to extract the relative phase value of dynamic path over the static path rather than sanitizing the phase value of static path as SpotFi [8] did. Furthermore, it is more challenging than the passive acoustic sensing with smart phone [24] due to presence of the CFO.

5 SYSTEM DESIGN

Figure 11 illustrates the system architecture of our prototype to detect hand movement that is environment and time independent using COTS WiFi devices with no training requirements. The system is composed of two stages, static CSI profiling stage and motion tracking stage.

5.1 Static CSI Profiling Stage

The upper three boxes in the left column of Figure 11 comprise the static CSI profiling stage. This stage is conducted under a static environment during which CSI is stable. Enough samples of (static) CSI are first collected and phase calibration is done by using method of SpotFi [8] that deals with only the static paths. Finally, the average value is calculated to reduce both the amplitude and phase noise.

5.2 Motion Tracking Stage

The right column of Figure 11 illustrates the motion tracking stage. This stage is comprised of CSI sample collection in a dynamic environment, denoising the raw CSI amplitude, detecting hand movement by analyzing phase difference between the subcarriers, and finally, extracting the dynamic path CSI corresponding to the hand by taking into account the static CSI profile. After finding the dynamic path CSI, we use the well-known MUSIC algorithm [14] to identify the AoA changes of hand.

Denoising raw CSI amplitude: The original CSI is extremely noisy. This noise is due to internal state changes, such as transmission power change. The noise is also on amplitude, which makes it hard to find the amplitude peaks and valleys. We could use a low pass or PCA filter as is done in [10, 23]. However, it will greatly distort the sinusoid wave shape of the amplitude over time. Instead, we use the Savitzky-Golay filter twice to double smooth the amplitude. This filter can smooth amplitude signal without greatly shifting the peak and valley points.

Detecting hand movement with phase difference: We use the average phase difference between the two receiver antennas as the indicator of hand movement. We set a threshold, and if the phase difference has fluctuations larger then the threshold, we assume that there is hand movement and start our dynamic path CSI extraction algorithm.

Extracting dynamic path CSI from measured CSI: WiDeo [7] uses full duplex technology to cancel interference from strong static signals. Such technology is not available in COTS WiFi. If the static reflections are stronger than the reflections from the moving object by more than the dynamic range of the radio, all information about the moving object will be lost in the quantization error of the ADC at the receiver. In order to eliminate the strong static path, our method extracts the dynamic path CSI value from the measured CSI with a pre-measured static CSI, which is described in the previous section 4.

Estimating the direction of hand movement: After finding the dynamic path CSI, we use the well-known MUSIC Algorithm [14] to identify the AoA changes due to hand movement. Since we use a spatial smoothing method to measure different dynamic paths, the path corresponding to hand is the one that changes AoA most rapidly. We do not use the SFO value for the purpose of localizing the hand position, as we only have the relative SFO change value rather than the absolute SFO value. We assume that during the segmentation, the speed of hand movement is constant.

5.3 Tracking Hand Movement

Now we explain how to estimate the movement of hand through AoA of the dynamic path reflected by hand. To map the direction (two dimensional) change to hand movement, we add another receiver and get the AoA for that receiver. In this case, the intersection of two AoAs is the position of hand. We can track hand movement by tracking this intersection point.

6 IMPLEMENTATION AND EVALUATION

We implemented our system using off-the-shelf Intel 5300 WiFi NICs (Figure 12). We employed the Linux CSI tool [5] to obtain the PHY layer CSI information for each packet. The Intel 5300 has three antennas and we place them linearly $\lambda/2$ apart. We set the channel to 40 MHz at a 5GHz frequency, which is the maximum we could set for Intel 5300 NIC. The CSI tool provides the user CSI values of 30 subcarriers spread over 120 subcarriers of 40MHz bandwidth. In our system we do not require any modification of the existing WiFi standard. We only monitor the signals of the incoming packets and analyze these signals.

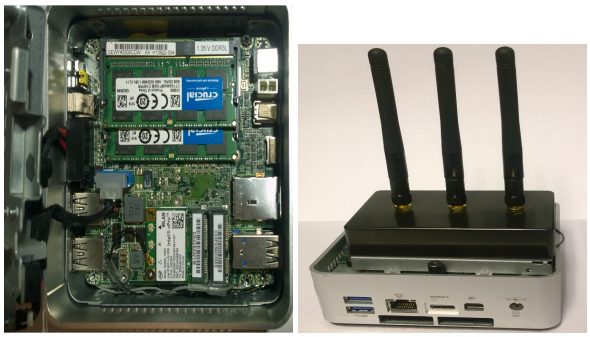

(a) Intel 5300 NICs (b) Intel 5300 with three antennas

Figure 12: Intel NUC with off-the-shelf Intel 5300 WiFi NICs

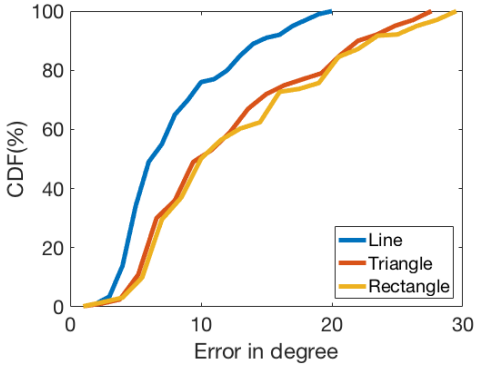

Figure 13: Angle error for LOS

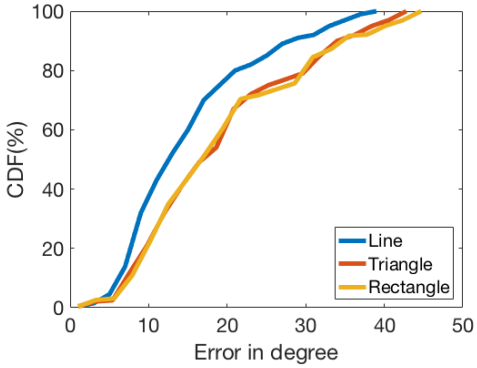

Figure 14: Angle error for NLOS

6.1 Experiment set up

We set the experiment with two receivers and one transmitter. This is a practical setup for an indoor environment such as a home where there are typically some nodes that stay in a stable location, e.g. the two receivers could be the access point and the smart TV and the transmitter could be any other wireless node. We evaluate our algorithm via three different types of hand motions: straight lines by moving the hand in one direction, triangles by moving the hand to make a triangle, and rectangles by moving the hand to make a shape as shown in Figure 21 (dotted lines). We use pre-defined templates as the ground truth. Each template is drawn on a table, and the hand is moving on the table accordingly. This means there is a possibility of extra error when the hand movement does not follow the template exactly. In all our experiments, the two receivers are placed 1 meter apart in a known location and the person is siting 1 meter away from both of these receivers.

We create two wireless node deployment strategies: Light-of-Sight (LOS) and Non-light-of-Sight (NLOS). For LOS scenario, we put the transmitter and the two receivers on the same side of wall, so there is no blocking of the direct-path. For NLOS scenario, we put the receivers on the same side of wall with human while the transmitter is on the other side of the wall, so that the direct paths have go through a wall, and the power of the direct path and the reflection path will be weaker compared to the LOS case.

We use a threshold in phase difference change to detect whether there is a hand movement or not for trigging our hand tracking system. Our experiments shows that we have 99.8% accuracy detecting whether there is a hand movement or not.

6.2 Experimental results

Angle accuracy. Figures 13 and 14 show the CDF of the error in angle measurement compared to the ground truth for LOS and NLOS scenarios respectively. We see that straight line hand movement has an average error of five degrees, and achieves 80th percentile angle estimation error up to 14 degrees. For triangle and rectangle movements, the average error is increased to ten degrees. The main reason for this increase is that when we draw complex shapes, the hand moves in more than one line which causes more multi-path interference.

Tracking Accuracy. Figures 15 and 16 show the CDF of the error in location measurement compared to the ground truth template for LOS and NLOS scenarios respectively. We see that the straight line hand movement has an average error of 8 cm, and achieves 80th percentile tracking error up to 15 cm. As with the straight line movement, for triangle and rectangle movements, the average error is slightly increased. The reason for this increase is the same as that for straight line, i.e. when we draw complex shapes, the hand moves in more than a single line, which causes more multi-path interference.

Impact of hand movement speed. The speed of the hand moving is expected to have impact on angle and tracking accuracy performance. As the hand moves faster, fewer samples are available to track the hand. For a particular hand movement, by measuring the path length change divided by the number of samples, we can estimate the speed of our hand movement. We define (30 cm/1000 samples) as the normal speed, (30 cm/500 samples) as the fast speed, and (30 cm/2000 samples) as the slow speed. Figures 17 and 18 show the angle error and tracking error respectively for the three different speeds for straight line hand movement (slow, normal, and fast speed). We notice that the accuracy increases as the speed of hand movement decreases. Accuracy is significantly increased from quick speed movement to normal speed movement, while the improvement from normal speed to the slow speed is small. So as long as the the hand moving speed is not too quick, the performance

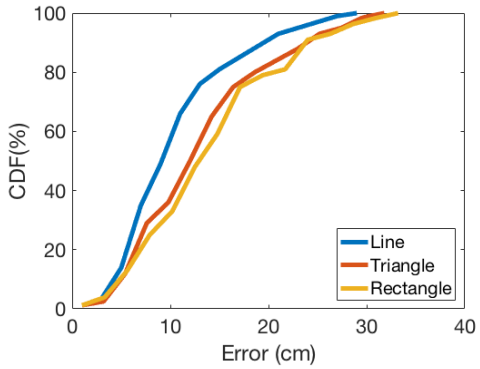

Figure 15: Tracking error for LOS

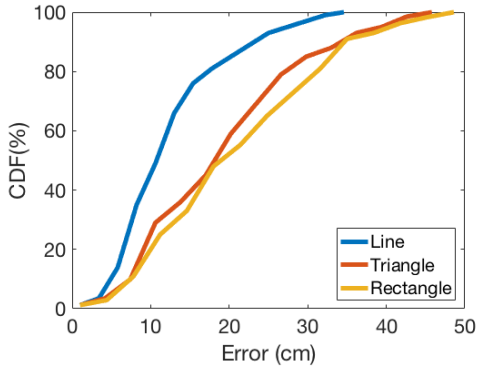

Figure 16: Tracking error for NLOS

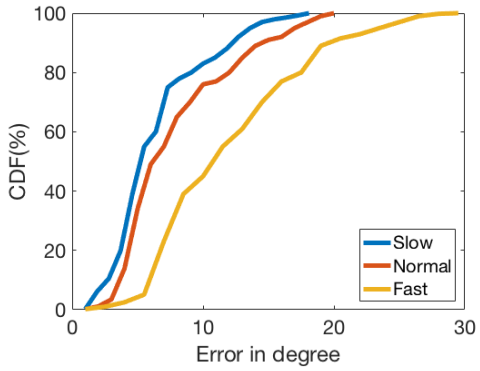

Figure 17: Angle error for different speed

is is quite good. Accuracy performance improvement gets smaller for lower speeds because the error in those situations arise mostly from the multi-path interference from hand movement.

Improvement with phase difference. One interesting question is that how much the phase difference contributes to overall accuracy of the algorithm. Figures 19 shows the improvement with and without the the phase difference of measured CSI while drawing a line. The solid lines represent the CDF of error in angle while the dash lines represent the CDF of error in location. We see that

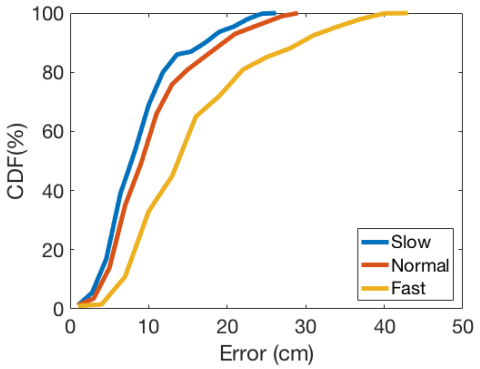

Figure 18: Tracking error for different speed

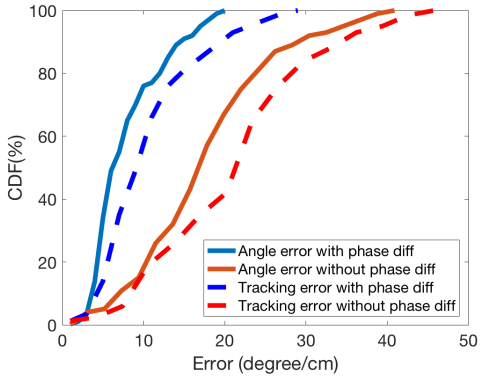

Figure 19: Error improvements with phase difference.

there is significant accuracy improvement in hand tracking if we consider the phase difference. The scheme without phase noise is totally based on the amplitude in calculating the dynamic path CSI. It could only achieve 80th percentile tracking error up to 30 cm, which is not enough for tracking the hand movement.

Environment independence: Since our algorithm extracts the calibrated hand movement on the dynamic path from the measured CSI, we can eliminate the difference introduced from the different static environments. To evaluate environment independence, we set up the same experiment in three different types of locations, one in home, one in a conference room, and the third in a classroom (See Figure 20). In all experiments, we performed the same hand movement relative to the receivers.

In our experiments, we mainly focused on measuring angle and tracking errors. We used the tool *Myscript* to detect the shape of hand movements. Figure 21 also shows the snapshots of this recognition. Average errors ranged from 5 to 10 degrees for angles and 8 to 16 cm for tracking. It is important to note that these errors are low enough that it is straight forward to detect the hand movements such as straight line, triangle or rectangle with a very high (nearly 100%) accuracy. Figure 22 shows the recognition rate in the there different locations we tested, assuring that the algorithm is robust to environmental changes.

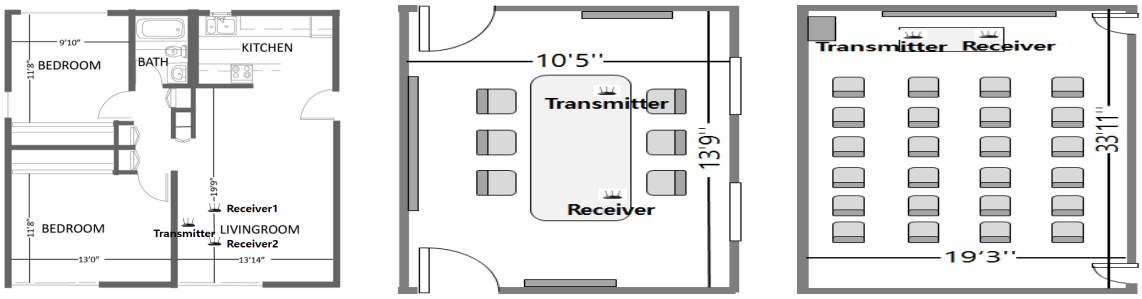

(a) Home apartment (b) Conference room (c) Classroom

Figure 20: Floor plans of three different types of locations.

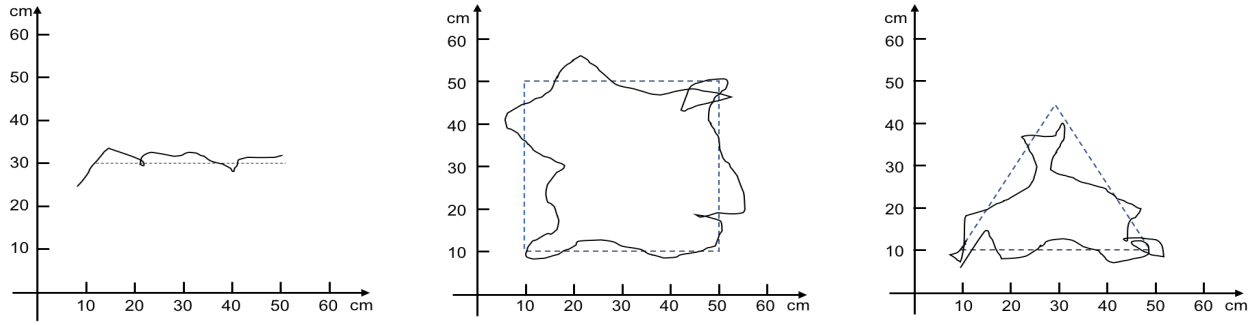

(a) Draw line (b) Draw rectangle (c) Draw triangle

Figure 21: Sample results of draw.

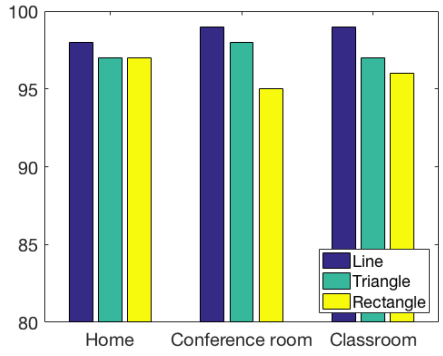

Figure 22: Hand movement recogniton.

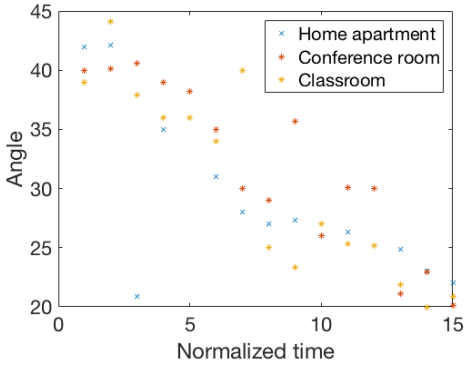

Figure 23: Hand direction tracking.

We also tested the tracking angle from one receiver, which is shown in Figure 23. As we can see, in all hand movements, we can identify that the AoA of the hand in one of receiver moves from approximately 41-42 degree to around 20-23 degree. This observation indicates that our algorithm can eliminate enough static-path power to identify hand tracking and works well independent of the environment.

7 DISCUSSION

The accuracy of hand motion tracking using our algorithm has some limitations, especially when other parts of the body move along with hand movement. The multi-path caused by other parts of body movement will affect the wave shape of the amplitude. As a result, the assumption that the amplitude of the maximum point is constructed by the in-phase of the static path and the dynamic path may not hold. In our future work, we will address this limitation.

8 CONCLUSIONS

In this paper, we present a new phase noise calibration technique for fine-grained motion tracking using COTS WiFi. This methodology is non-intrusive, time and environment independent, and does not require any training. The major obstacle in using the COTS WiFi for advanced wireless sensing technology is the WiFi NIC's frequency unlocked oscillator, which introduces sampling frequency offset and carrier frequency offset that cause too much noise in phase when extracting motion from the CSI. We leverage the phenomenon of sinusoid wave on amplitude and phase values upon the dynamic path length change which happens when there is a movement. We first extract the amplitude of dynamic path and the triangle relationship of measured CSI, static path CSI vector and dynamic path CSI vector to remove phase noise and calibrate the CFO of the CSI for dynamic path. Then we compute the dynamic path CSI using the estimated CFO. We have developed a prototype system based on this methodology. Experimental evaluation shows that this prototype can detect hand movements, and distinguish between different types of movements quite accurately.

ACKNOWLEDGMENTS

We thank Mohammad Hashemi for the experiments and discussion, and the reviewers for their insightful comments.

REFERENCES

[1] http://www.microsoft.com/en-us/kinectforwindows/.
[2] F. Adib, Z. Kabelac, D. Katabi, and R. C. Miller. 3d tracking via body radio reflections. In *Proceedings of the 11th USENIX Conference on Networked Systems Design and Implementation*, NSDI'14, pages 317–329, Berkeley, CA, USA, 2014. USENIX Association.
[3] F. Adib and D. Katabi. See through walls with wifi! In *Proceedings of the ACM SIGCOMM 2013 Conference on SIGCOMM*, SIGCOMM '13, pages 75–86, New York, NY, USA, 2013. ACM.
[4] C. An, T. Li, Z. Tian, A. T. Campbell, and X. Zhou. Visible light knows who you are. In *Proceedings of the 2Nd International Workshop on Visible Light Communications Systems*, VLCS '15, pages 39–44, New York, NY, USA, 2015. ACM.
[5] D. Halperin, W. Hu, A. Sheth, and D. Wetherall. Tool release: Gathering 802.11n traces with channel state information. *SIGCOMM Comput. Commun. Rev.*, 41(1):53–53, Jan. 2011.
[6] F. A. Jenkins and H. E. White. *Fundamentals of optics*. Tata McGraw-Hill Education, 1957.
[7] K. Joshi, D. Bharadia, M. Kotaru, and S. Katti. Wideo: Fine-grained device-free motion tracing using rf backscatter. In *Proceedings of the 12th USENIX Conference on Networked Systems Design and Implementation*, NSDI'15, pages 189–204, Berkeley, CA, USA, 2015. USENIX Association.
[8] M. Kotaru, K. Joshi, D. Bharadia, and S. Katti. Spotfi: Decimeter level localization using wifi. In *Proceedings of the 2015 ACM Conference on Special Interest Group on Data Communication*, SIGCOMM '15, pages 269–282, New York, NY, USA, 2015. ACM.
[9] J. Liu, Y. Wang, Y. Chen, J. Yang, X. Chen, and J. Cheng. Tracking vital signs during sleep leveraging off-the-shelf wifi. In *Proceedings of the 16th ACM International Symposium on Mobile Ad Hoc Networking and Computing*, MobiHoc '15, pages 267–276, New York, NY, USA, 2015. ACM.
[10] J. Liu, Y. Wang, G. Kar, Y. Chen, J. Yang, and M. Gruteser. Snooping keystrokes with mm-level audio ranging on a single phone. In *Proceedings of the 21st Annual International Conference on Mobile Computing and Networking*, MobiCom '15, pages 142–154, New York, NY, USA, 2015. ACM.
[11] W. Mao, J. He, and L. Qiu. Cat: High-precision acoustic motion tracking. In *Proceedings of the 22Nd Annual International Conference on Mobile Computing and Networking*, MobiCom '16, pages 69–81, New York, NY, USA, 2016. ACM.
[12] L. Motion. https://www.leapmotion.com/.
[13] R. Nandakumar, V. Iyer, D. Tan, and S. Gollakota. Fingerio: Using active sonar for fine-grained finger tracking. In *Proceedings of the 2016 CHI Conference on Human Factors in Computing Systems*, CHI '16, pages 1515–1525, New York, NY, USA, 2016. ACM.
[14] R. O. Schmidt. *Multiple emitter location and signal parameter estimation*. IEEE Transactions on Antennas and Propagation, AP-34(3):276–280, 1986.
[15] S. Sen, B. Radunovic, R. R. Choudhury, and T. Minka. You are facing the mona lisa: Spot localization using phy layer information. In *Proceedings of the 10th International Conference on Mobile Systems, Applications, and Services*, MobiSys '12, pages 183–196, New York, NY, USA, 2012. ACM.
[16] L. Sun, S. Sen, D. Koutsonikolas, and K.-H. Kim. Widraw: Enabling hands-free drawing in the air on commodity wifi devices. In *Proceedings of the 21st Annual International Conference on Mobile Computing and Networking*, MobiCom '15, pages 77–89, New York, NY, USA, 2015. ACM.
[17] D. Vasisht, S. Kumar, and D. Katabi. Decimeter-level localization with a single wifi access point. In *13th USENIX Symposium on Networked Systems Design and Implementation (NSDI 16)*, pages 165–178, Santa Clara, CA, 2016. USENIX Association.
[18] H. Wang, T. T.-T. Lai, and R. Roy Choudhury. Mole: Motion leaks through smartwatch sensors. In *Proceedings of the 21st Annual International Conference on Mobile Computing and Networking*, MobiCom '15, pages 155–166, New York, NY, USA, 2015. ACM.
[19] H. Wang, D. Zhang, J. Ma, Y. Wang, Y. Wang, D. Wu, T. Gu, and B. Xie. Human respiration detection with commodity wifi devices: Do user location and body orientation matter? In *Proceedings of the 2016 ACM International Joint Conference on Pervasive and Ubiquitous Computing*, UbiComp '16, pages 25–36, New York, NY, USA, 2016. ACM.
[20] J. Wang, H. Jiang, J. Xiong, K. Jamieson, X. Chen, D. Fang, and B. Xie. Lifs: Low human-effort, device-free localization with fine-grained subcarrier information. In *Proceedings of the 22Nd Annual International Conference on Mobile Computing and Networking*, MobiCom '16, pages 243–256, New York, NY, USA, 2016. ACM.
[21] J. Wang, D. Vasisht, and D. Katabi. Rf-idraw: Virtual touch screen in the air using rf signals. In *Proceedings of the 2014 ACM Conference on SIGCOMM*, SIGCOMM '14, pages 235–246, New York, NY, USA, 2014. ACM.
[22] W. Wang, A. X. Liu, and M. Shahzad. Gait recognition using wifi signals. In *Proceedings of the 2016 ACM International Joint Conference on Pervasive and Ubiquitous Computing*, UbiComp '16, pages 363–373, New York, NY, USA, 2016. ACM.
[23] W. Wang, A. X. Liu, M. Shahzad, K. Ling, and S. Lu. Understanding and modeling of wifi signal based human activity recognition. In *Proceedings of the 21st Annual International Conference on Mobile Computing and Networking*, MobiCom '15, pages 65–76, New York, NY, USA, 2015. ACM.
[24] W. Wang, A. X. Liu, and K. Sun. Device-free gesture tracking using acoustic signals. In *Proceedings of the 22Nd Annual International Conference on Mobile Computing and Networking*, MobiCom '16, pages 82–94, New York, NY, USA, 2016. ACM.
[25] T. Wei and X. Zhang. mtrack: High-precision passive tracking using millimeter wave radios. In *Proceedings of the 21st Annual International Conference on Mobile Computing and Networking*, MobiCom '15, pages 117–129, New York, NY, USA, 2015. ACM.
[26] D. Wu, D. Zhang, C. Xu, Y. Wang, and H. Wang. Widir: Walking direction estimation using wireless signals. In *Proceedings of the 2016 ACM International Joint Conference on Pervasive and Ubiquitous Computing*, UbiComp '16, pages 351–362, New York, NY, USA, 2016. ACM.
[27] L. Yang, Y. Chen, X.-Y. Li, C. Xiao, M. Li, and Y. Liu. Tagoram: Real-time tracking of mobile rfid tags to high precision using cots devices. In *Proceedings of the 20th Annual International Conference on Mobile Computing and Networking*, MobiCom '14, pages 237–248, New York, NY, USA, 2014. ACM.
[28] L. Yang, Q. Lin, X. Li, T. Liu, and Y. Liu. See through walls with cots rfid system! In *Proceedings of the 21st Annual International Conference on Mobile Computing and Networking*, MobiCom '15, pages 487–499, New York, NY, USA, 2015. ACM.